Original scientific paper

Informacije MIDEM
Journal of Microelectronics,
Electronic Components and Materials
Vol. 48, No. 2(2018), 97 – 113

Lossy and Lossless Inductance Simulators and Universal Filters Employing a New Versatile Active Block

Mohammad Faseehuddin[1], Jahariah Sampe[2], Sadia Shireen[3], Sawal Hamid Md Ali[4]

[1]Institute of Microengineering and Nanoelectronics (IMEN),UniversityKebangsaan Malaysia (UKM), Bangi, Selangor, Malaysia
[2]Institute of Microengineering and Nanoelectronics (IMEN), University Kebangsaan Malaysia (UKM), Bangi, Selangor, Malaysia
[3]Department of Electronics and Communication, Indus Institute of Technology and Management, Kanpur, India
[4]Department of Electrical, Electronic and Systems Engineering, Universiti Kebangsaan Malaysia, Bangi, Selangor, Malaysia

Abstract: In this paper six new implementations for realizing lossy and lossless active inductors are presented. The new topologies are obtained using a newly formulated active block namely, the extra X current conveyor transconductance amplifier (EXCCTA). The designed grounded inductor simulators (GIS) require only three grounded passive elements for implementation which is desirable for integrated circuit fabrication. Moreover, the inductance simulators are electronically tunable and free from matching requirements. Additionally, two structures of universal filters are also proposed. The voltage mode (VM) filter is multi input single output (MISO) structure and uses canonical number of passive components. The current mode (CM) filter is a single input multi output (SIMO) structure with grounded passive elements. The filter structures can realize all five standard filter responses without any matching conditions and have features of low/ high output impedance, low active and passive sensitivities, tunability, independent control of pole frequency and quality factor. The effect of non-idealities on the inductor and filter topologies are also analyzed. The simulations are performed in 0.18µm parameters from TSMC in Spice to validate the theoretical predictions. Experimental results using AD844 and LM13700 integrated circuits (ICs) for the proposed inductor and filter are also provided to further ascertain the feasibility of the proposed solutions.

Keywords: active inductor; current mode; current conveyor; filter; tunability

Izgubni in brezizgubni induktivni simulator ter univerzalen filter z z novim prilagodljivim aktivnim blokom

Izvleček: Članek predstavlja šest primerov realizacije izgubnih in brez izgubnih aktivnih dušilk. Nove topologije uporabljajo nov aktivni blok; ekstra X tokovni transkonduktančni ojačevalnik (EXCCTA). Načrtani ozemljeni induktivni simulatorji (GIS) zahtevajo le tri ozemljene pasivne elemente in so elektronsko nastavljivi ter neodvisni od zahtev ujemanja. Dodatno sta predlagani dve strukturi univerzalnega filtra. Več vhodni in eno izhodni filter v napetostnem načinu uporablja standardno število pasivnih elementov. Tokovni filter je eno vhodni in več izhodni z ozemljenimi elementi. Filtri lahko realizirajo vseh pet standardnih odzivov brez prilagajanj. Imajo nizko/visoko izhodno impedanco, nizko aktivno in pasivno občutljivost, nastavljivost, neodvisno kontrolo frekvence in faktorja kvalitete. Simulacije so izvedene v 0.18 µm tehnologiji iz TSMC in SPICE za validacijo teoretičnih predvidevanj. Eksperimentalni rezultati so pridobljeni s uporabo AD844 in LM13700 integriranih vezij.

Ključne besede: aktivna dušilka; tokovni način; tokovni ojačevalnik; filter; nastavljivost

** Corresponding Author's e-mail: faseehuddin03@siswa.ukm.edu.my*

1 Introduction

The physical spiral inductors suffer from low realizable inductance value of the order of 1nH [1, 2], low quality factor, higher chip area requirement, excessive losses and susceptibility to process variations [1]. These drawbacks make them unsuitable for integrated circuit implementation. Since inductors are inevitable components given their broad spectrum of applications in active filters, parasitic cancellation, oscillators, radio frequency (RF) systems etc. [2]. The active simulation of inductors where active devices are employed instead of spiral inductors to emulated the behavior of passive inductors has become popular [1-3]. Analog filters are an integral part of almost every electronic system and so their synthesis and development remains an ever evolving field. Among various filter structures universal filters (UFs) are the most versatile as all the standard filter functions can be derived from them[6-9]. They serve as standalone solution to many filtering needs. The UFs find applications in phase locked loop FM stereo demodulator, telephone decoder, speech processing etc.[7-8]. The current mode active elements are the best choice for inductor and filter synthesis, owning to their large dynamic range, great linearity, wide bandwidth, higher slew rate and excellent low voltage performance compared to their voltage mode counterparts [6-7]. Numerous current mode active blocks have been employed for inductance simulation and filter design like second generation current conveyor (CCII) [4], differential voltage current conveyor (DVCCII) [2], dual X current conveyor (DXCCII) [22], current conveyor transconductance amplifier (CCTA) [28], differential current conveyor (DCCII) [11], differential difference current conveyor (DDCC) [1], fully differential current conveyor (FDCCII) [34], voltage differencing current conveyor (VDCC) [25], current feedback operational amplifier (CFOA) [13], modified current feedback operational amplifier (MCFOA) [18], inverting current feedback operational amplifier (CFOA-) [5], current differencing transconductance amplifier (CDTA) [37] etc.

The GIS can be categorized based on many criteria like number of active devices used, passive component count, lossy/lossless type inductance realization, use of grounded passive elements, feature of inbuilt tunability, capability of active element realization using the off the shelf integrated circuits (ICs) like AD844 etc. The GIS presented in [4, 12-13] require more than one active element for inductance simulation. The GIS implementations presented in [4, 12-13, 15, 21, 23] require more than three passive elements. Although in current fabrication technology it is feasible to implement floating capacitor but use of grounded capacitor has inherent advantages in terms noise cancelation, chip area and parasitic reduction. The GIS implementations in [5, 10, 12, 14-17, 19, 21-24] makes use of one or more floating capacitors. Tunability is one of the major design requirements in today's mixed mode systems. The GIS circuits in [1, 4-5, 11-24] did not have inbuilt tuning capability. A thorough comparison of the exemplary inductance topologies available in the literature with the proposed lossy/lossless GIS topologies is given in Table 1. The literature survey reveals that the draw backs of the majority of the presented inductor simulators are (i) no provision for on chip tunability (ii) use of more than one active element (iii) use of floating capacitor (iv) excessive use of passive elements (v) passive components matching requirnment.

In this research a new active block the extra X current conveyor transconductance amplifier (EXCCTA) is utilized in designing six topologies of lossy/lossless inductance simulators. All the designed GIS employ only a single active element and two/three grounded passive elements for implementation. No matching is required for implementation and inductance can be easily tuned via bias current of the transconductor. Further more, two minimum component VM and CM mode universal filters are proposed. The filters structures are characterized by following attributes (i) use of minimum number of active blocks and passive components (ii) inbuilt tunability (iii) use of grounded passive elements (iv) provision for independent control of pole frequency and quality factor (v) avalibility of output at low impedance in case of VM filter and high impedance in CM filter. The simulation are performed using 0.18µm parameters from TSMC in Spice to validate the theoretical findings. Additionally, an experimental study of pure inductor and VM SIMO filter is conducted using AD844 and LM13700 ICs. The measured results are compared with the ideal ones.

2 Extra X current conveyor transconductance amplifier (EXCCTA)

The proposed Extra X current conveyor transconductance amplifier (EXCCTA) is functionally a connection of extra x current conveyor (EXCCII) [26] and operational transconductance amplifier (OTA) [30]. The new block carries features of CCII and tunable OTA in a single integrated circuit structure. The Voltage current characteristics of the developed EXCCTA are given in matrix Equation1 and the block diagram is presented in Fig. 1. The block is found to be suitable for implementing minimum component filters and inductor simulators as it provides two independent current input X terminals and an inherent tunable structure.

Table 1: Comparison of exemplary active inductors with the proposed ones

Reference	No. of Active Devices Used	No. of Passive Elements	Capacitor Floating	Matching Condition	Inbuilt Tunability
[1] Fig. 5	MDO-DDCC (1)	3	No	Yes	No
[4]	CCII (3)	4	No	No	No
[5]	CFOA – (1)	3	Yes	No	No
[10]	VDBA (1)	2	Yes	No	Yes
[11]	DCCII (1)	3	No	Yes	No
[12]	OTRA (2)	5	Yes	Yes	No
[13]	CFOA (2)	4	No	Yes	No
[14]	DCCII (1)	3	Yes	No	No
[15]	OTRA (1)	4	Yes	No	No
[16]	MICCII (1)	3	Yes	Yes	No
[17]	GVCCIII (1)	3	Yes	Yes	No
[18]	MCFOA (1)	3	No	No	No
[19]	CFOA (1)	3	Yes	No	No
[20]	CCII (1)+Current Follower (1)	3	No	No	No
[21]	PFTN (1)	5	Yes	Yes	No
[22]	DXCCII (1)	3	Yes	Yes	No
[23]	OTRA (1)+Voltage Buffer (1)	4	Yes	Yes	No
[24]	CFOA (1)	3	Yes	No	No
Fig. 3 Proposed GIS-(1-2, 4-6)	EXCCTA (1)	3	No	No	Yes
Fig. 3 Proposed GIS-3	EXCCTA (1)	2	No	No	Yes

$$\begin{bmatrix} I_Y \\ V_{XP} \\ V_{XN} \\ I_{ZP+} \\ I_{ZP-} \\ I_{ZN+} \\ I_{ZN-} \\ I_{0+} \end{bmatrix} = \begin{bmatrix} 0 & 0 & 0 & 0 & 0 & 0 & 0 & 0 \\ 1 & 0 & 0 & 0 & 0 & 0 & 0 & 0 \\ 1 & 0 & 0 & 0 & 0 & 0 & 0 & 0 \\ 0 & 1 & 0 & 0 & 0 & 0 & 0 & 0 \\ 0 & -1 & 0 & 0 & 0 & 0 & 0 & 0 \\ 0 & 0 & 1 & 0 & 0 & 0 & 0 & 0 \\ 0 & 0 & -1 & 0 & 0 & 0 & 0 & 0 \\ 0 & 0 & 0 & g_m & 0 & 0 & 0 & 0 \end{bmatrix} \begin{bmatrix} V_Y \\ I_{XP} \\ I_{XN} \\ V_{ZP+} \\ V_{ZP-} \\ V_{ZN+} \\ V_{ZN-} \\ V_O \end{bmatrix} \quad (1)$$

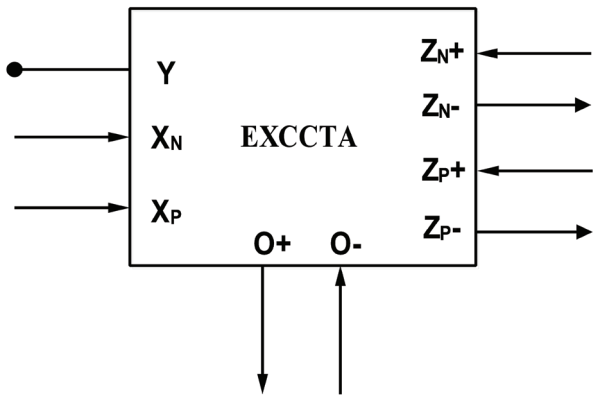

Figure 1: Block diagram of EXCCTA

The CMOS implementation of EXCCTA is presented in Fig. 2. It is a 9 terminal active element. The first stage consists of EXCCII transistors (M1-M28). The voltage applied at Y node appears at XP and XN nodes. The current input at X_p node is transferred to nodes Z_{p+} and Z_{p-}. In the same way the input current from X_N node is transferred to Z_{N+} and Z_{N-}. The current following in Z_N and Z_p terminals are independent of each other. The class AB output stage is selected for the implementation as it is suitable for low voltage operation [6]. The second stage is composed of OTA. The transconductance is realized using transistors (M29-M40).The output current of the trans-conductor depends on the voltage Z_{p+}. Assuming saturation region operation for all transistors and equal W/L ratio for transistors M29 and M30 the output current I_o of the OTA is given by Equation 2.

$$I_O = g_{mi}\left(V_{ZP+}\right) = \left(\sqrt{2I_{Bias}K_i}\right)\left(V_{ZP+}\right) \quad (2)$$

Where, the transconductance parameter $K_i = \mu C_{0x} W/2L$, (i=29, 30) W is the effective channel width, L is the effective length of the channel, C_{ox} is the gate oxide capacitance per unit area and μ is the carrier mobility. It is evident from (2) that the transconductance can be tuned by the bias current thus imparting tunability to the structure.

The most critical parameters of the EXCCTA can be computed by following the analysis procedure given in

[6]. The voltage transfer ratio between Y and X_p node can be derived as given in Equation 3.

$$\alpha_P = \frac{V_{XP}}{V_Y} = \frac{\frac{r_{09}r_{014}}{r_{09}+r_{014}}\left(g_{m9}+g_{m14}\right)\frac{r_{0p}}{2}g_{m4}}{\frac{r_{09}r_{014}}{r_{09}+r_{014}}\left(g_{m9}+g_{m14}\right)\frac{r_{0p}}{2}g_{m3}+1} \cong \frac{g_{m4}}{g_{m3}} \quad (3)$$

Where $r_{0p} = r_{03}//r_{07}$, r_0 is the output resistance of the MOS transistor and g_m is the transconductance of the MOS transistor. In the similar way the voltage transfer between Y and X_N can be obtained as given below. The current transfer ratios β_p and β_N depend on the load connected at X and Z terminals. This is a slight draw back but if the value of the load connected is less than MOS transistor resistance than an accurate transfer is achieved. The current transfer ratios are derived as given in Equation 5-6.

$$\alpha_N = \frac{V_{XP}}{V_Y} \cong \frac{g_{m1}}{g_{m2}} \quad (4)$$

$$\beta_P = \frac{I_{ZP}}{I_{XP}} = \frac{\frac{\frac{r_{010}r_{015}}{r_{010}+r_{015}}(g_{m10}+g_{m15})}{\frac{r_{010}r_{015}}{r_{010}+r_{015}}(g_{m10}+g_{m15})+R_{ZLOAD}}}{\frac{\frac{r_{09}r_{014}}{r_{09}+r_{014}}(g_{m9}+g_{m14})}{\frac{r_{09}r_{014}}{r_{09}+r_{014}}\left(g_{m9}+g_{m14}\right)+R_{XLOAD}}} \cong \frac{g_{m10}+g_{m15}}{g_{m9}+g_{m14}} \quad (5)$$

$$\beta_N = \frac{I_{ZN}}{I_{XN}} \cong \frac{g_{m20}+g_{m24}}{g_{m19}+g_{m28}} \quad (6)$$

The X terminal resistance of X_N and X_p terminal is calculated as given in Equations 7-8.

$$R_{XP} = \frac{1}{\frac{r_{09}r_{014}}{r_{09}+r_{014}}+\left(g_{m9}+g_{m14}\right)\frac{r_{0p}}{2}g_{m4}} \cong \quad (7)$$

$$\cong \frac{2}{r_{0p}g_{m4}\left(g_{m9}+g_{m14}\right)}$$

$$R_{XN} \cong \frac{2}{r_{0n}g_{m1}\left(g_{m19}+g_{m28}\right)} \quad (8)$$

Where $r_{0p} = r_{03}//r_{07}$ and Where $r_{0n} = r_{02}//r_{06}$

The Z and O nodes impedances are found to be high given by parallel output resistance of MOS transistors.

$$R_{ZP} = \frac{r_{010}r_{015}}{r_{010}+r_{015}} \quad (9)$$

$$R_{ZN} = \frac{r_{020}r_{024}}{r_{020}+r_{024}} \quad (10)$$

$$R_{Z0+} = \frac{r_{033}r_{039}}{r_{033}+r_{039}} \quad (11)$$

The extra transistor count should not be considered a disadvantage since the unused Z terminal can be removed reducing the transistor count.

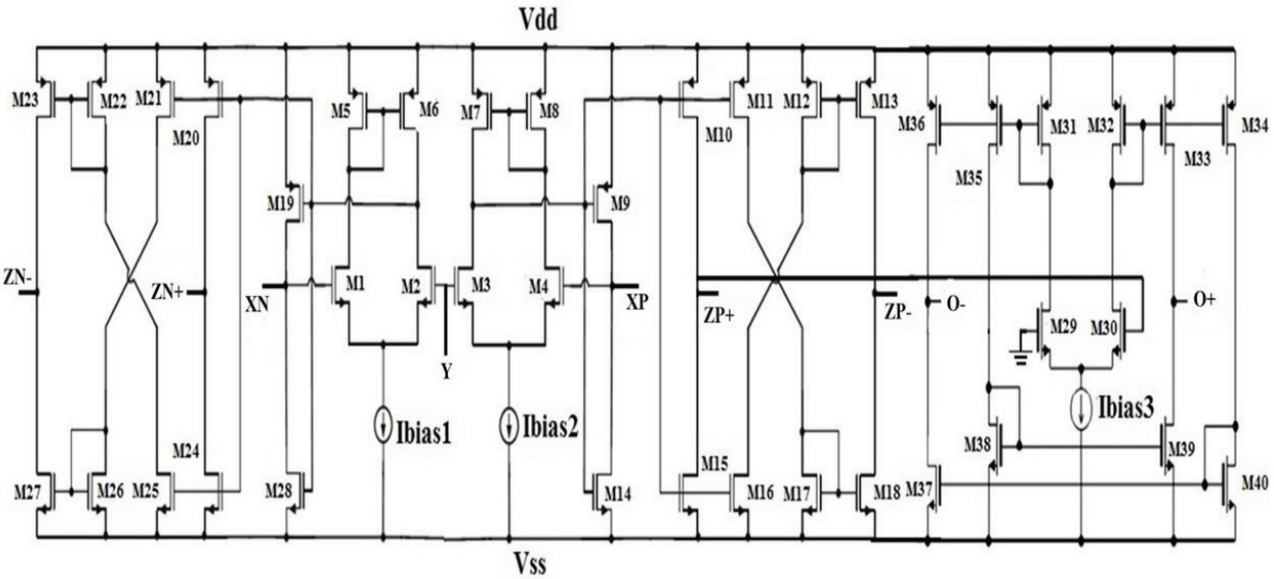

Figure 2: CMOS Implementation of EXCCTA

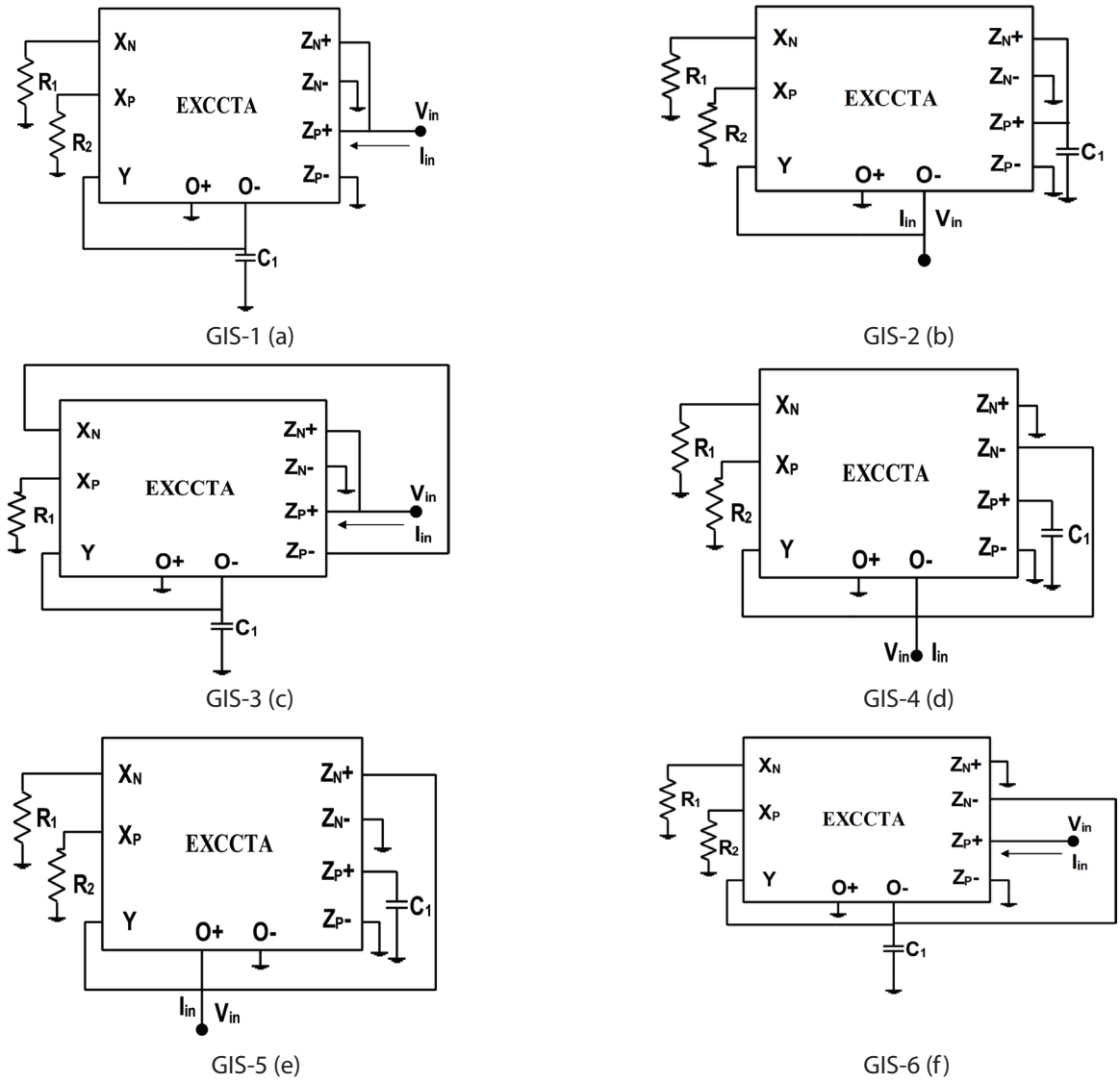

Figure 3: The proposed lossless and Lossy inductor simulators

Table 2: The impedance relations of the proposed active inductors

Simulator	Impedance Realized	Inductance (L_{eq})	Equivalent Resistance (R_{eq})	Type	Tunability	Matching Requirement
GIS-1	L_{eq}	$\frac{SC_1R_1R_2}{g_m(R_1+R_2)}$	-	Pure	Yes	No
GIS-2	L_{eq}	$\frac{SC_1R_1R_2}{g_m(R_1+R_2)}$	-	Pure	Yes	No
GIS-3	L_{eq}	$\frac{SC_1R_1}{2g_m}$	-	Pure	Yes	No
GIS-4	$\frac{1}{L_{eq}}+\frac{1}{R_{eq}}$	$\frac{SC_1R_2}{g_m}$	R_1	L in parallel with R	Yes	No
GIS-5	$-\frac{1}{L_{eq}}-\frac{1}{R_{eq}}$	$-\frac{SC_1R_2}{g_m}$	$-R_1$	-L in parallel with -R	Yes	No
GIS-6	$L_{eq}+R_{eq}$	$\frac{SC_1R_2}{g_m}$	$\frac{R_2}{R_1g_m}$	L in series with R	Yes	No

3 The proposed inductor simulators and universal filters

The proposed inductor simulators using a single EXCCTA and grounded passive elements are shown in Fig. 3(a-f). A simple analysis of the circuits reveals that the GIS-1 to GIS-3 realize pure inductance. The GIS-4 and GIS-5 implements lossy parallel RL inductors. It is noteworthy that the value of the parallel resistor in GIS-4/5 can be set using resistor R_1 independent of the inductance value that is set by R_2 and g_m which is an advantage. Finally, the GIS-6 realizes lossy series RL inductor. The series resistance in GIS-6 can be altered by changing R_1 without affecting the inductance.

All the presented inductor simulators use only grounded passive elements which is advantageous for integrated circuit implementation. The use of grounded capacitor saves chip area and also minimizes noise effects. Furthermore, all the simulators are free from components matching constraints and tunable via bias current of the OTA. The impedance relations of the inductors are given in Table 2.

Next, the proposed VM universal filter is presented in Fig. 4. The filter structure is obtained by modifying the proposed series inductor GIS-6. The SIMO filter uses canonical number of passive components and can realize low pass (LP), high pass (HP), band pass (BP), notch pass (NP) and all pass (AP) responses. Among the two capacitors one is always grounded which is an advantage. The features of the filter includes use of single active block, low output impedance, tunability and provision for independent control of quality factor and pole frequency. The transfer function, expression of -3dB cutoff frequency, quality factor and bandwidth of the filter are given in Equations 12-14. The output can be tapped from Y terminal or low impedance X_N terminal. The combination of filter input modes and applied input voltages for realizing all the five filter responses is summarized in Table 3.

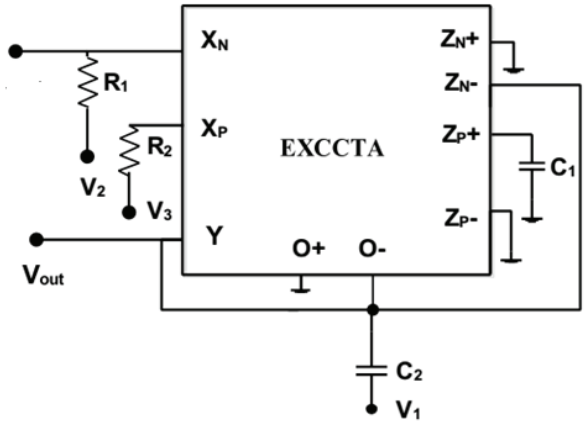

Figure 4: The proposed VM mode MISO filter

$$V_{out} = \frac{\frac{S^2C_1C_2R_2}{g_m}V_1 + \frac{SC_2R_2}{g_mR_1}V_2 + V_3}{\frac{S^2C_1C_2R_2}{g_m} + S\frac{C_2R_2}{g_mR_1} + 1} \quad (12)$$

$$\omega_o = \sqrt{\frac{g_m}{C_1C_2R_2}} \quad (13)$$

$$Q = R_1\sqrt{\frac{C_1g_m}{C_2R_2}} \quad (14)$$

Table 3: The activation sequence of the filter

Response	Inputs		
	V_1	V_2	V_3
LP	0	0	1
HP	1	0	0
BP	0	1	0
NP	1	0	1
AP	1	-1	1

The MISO CM filter is shown in Fig. 5. The filter employs three grounded passive elements and can realize all LP, BP and HP responses simultaneously. The AP response can be obtained by summing the HP, BP and LP responses. All the responses are available at high impedance nodes except the HP response which is available through the capacitor . The HP current can be sensed using a simple current follower. The features of the filter includes use of single active element, grounded passive elements and tunability. The transfer functions for five filter responses are given in Equations 15(a)-15(e).

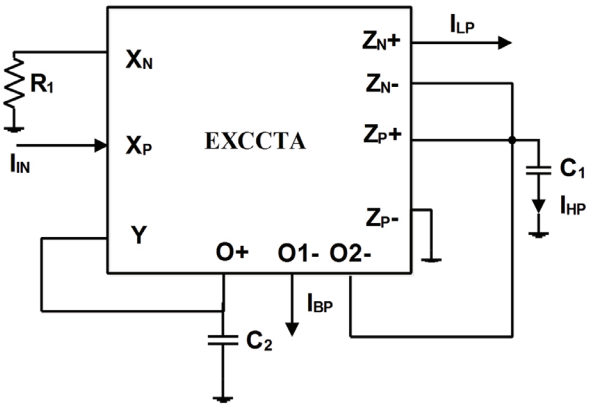

Figure 5: The proposed CM SIMO filter

$$\frac{I_{LP}}{I_{in}} = \frac{-1}{\frac{S^2C_1C_2R_1}{g_m} + SC_2R_1 + 1} \quad (15a)$$

$$\frac{I_{HP}}{I_{in}} = \frac{-\frac{S^2C_1C_2R_1}{g_m}}{\frac{S^2C_1C_2R_1}{g_m} + SC_2R_1 + 1} \quad (15b)$$

$$\frac{I_{BP}}{I_{in}} = \frac{SC_2R_1}{\frac{S^2C_1C_2R_1}{g_m} + SC_2R_1 + 1} \quad (15c)$$

$$\frac{I_{NP}}{I_{in}} = \frac{-1-\frac{S^2C_1C_2R_1}{g_m}}{\frac{S^2C_1C_2R_1}{g_m} + SC_2R_1 + 1} \quad (15d)$$

$$\frac{I_{AP}}{I_{in}} = \frac{-1-\frac{S^2C_1C_2R_1}{g_m} + SC_2R_1}{\frac{S^2C_1C_2R_1}{g_m} + SC_2R_1 + 1} \quad (15e)$$

$$f_o = \frac{1}{2\pi}\sqrt{\frac{g_m}{C_1C_2R_1}} \quad (16)$$

$$Q = \sqrt{\frac{C_1}{g_mC_2R_1}} \quad (17)$$

4 Non-Ideal analysis

In this section the Non-idealities of the EXCCTA are considered and their influence on the proposed inductors and filter circuits is analyzed. A simplified non-ideal model of EXCCTA is presented in Fig. 6 for analysis. The most important aspects contributing to the deviations in frequency performance are the non-ideal frequency dependent current and voltage transfer gains, $\alpha_i(s)$ and $\beta_i(s)$ respectively, where $\alpha_i(s) = \alpha_{0i}/(1 + s/\omega_{\alpha i})$ and $\beta_i(s) = \beta_{0i}/(1 + s/\omega_{\beta i})$. Ideally, $\alpha_{0i} = \beta_{0i} = 1$ and $\omega_{\alpha i} = \omega_{\beta i} = \infty$. Another important performance parameter is the associated parasitics at the X nodes which can be quantified as $Z_{XP} = Z_{XN} = R_{X(N,P)} + sL_{X(N,P)}$. The parasitic resistance and capacitance associated with the Y and Z nodes are R_{ZP}, R_{ZN} and R_Y. While the associated capacitances are C_{ZP}, C_{ZN} and C_Y. There ideal values being equal to zero.The γ represents the transconductance transfer inaccuracy of the OTA, while R_o and C_o are parasitics at the OTA output. If the effect of the non-ideal gains is considered the V-I relations of the EXCCTA will be modified to $I_Y = 0$, $V_{XP} = \beta_p(s)V_Y$, $V_{XN} = \beta_N(s)V_Y$, $I_{ZP+} = \alpha_p(s)I_{XP}$, $I_{ZP-} = \alpha_p'(s)I_{XP}$, $I_{ZN+} = \alpha_N(s)I_{XN}$, $I_{ZN-} = \alpha_N'(s)I_{XN}$, $I_{0+} = \gamma g_m V_{ZP+}$, $I_{0-} = \gamma' g_m V_{ZP+}$.

The modified expressions of inductance L_{eq} of the active inductor simulators taking into account the non-ideal current and voltage transfer gains of the EXCCTA is given in Table 4.

Table 4: Modified inductance L_{eq} of the active inductor simulators for non-ideal case

GIS-1	$L_{eq} = \frac{SC_1R_1R_2}{\gamma' g_m(\alpha_P\beta_PR_1 + \alpha_N\beta_NR_2)}$
GIS-2	$L_{eq} = \frac{SC_1R_1R_2}{\gamma' g_m(\alpha_P\beta_PR_1 + \alpha_N\beta_NR_2)}$
GIS-3	$L_{eq} = \frac{SC_1R_1}{\gamma' g_m(\alpha_P\beta_P + \alpha_N\beta_N)}$
GIS-4	$L_{eq} = \frac{\gamma' g_m\alpha_P\beta_P}{SC_1R_2} + \frac{\alpha_N'\beta_N}{R_1}$
GIS-5	$L_{eq} = \frac{-\gamma g_m\alpha_P\beta_P}{SC_1R_2} - \frac{\alpha_N\beta_N}{R_1}$
GIS-6	$L_{eq} = \frac{SC_1R_2}{\alpha_P\beta_P\gamma' g_m} + \frac{\alpha_N\beta_NR_2}{\gamma' g_mR_1}$

The expressions of transfer function, pole frequency and quality factor including the non-ideal gains for the VM and CM filters are presented in Equations 18-23, respectively.

$$V_{out} = \frac{\frac{S^2C_1C_2R_2}{\gamma g_m}V_1 + \frac{\alpha_N SC_2R_2}{\gamma g_mR_1}V_2 + \alpha_P\gamma V_3}{\frac{S^2C_1C_2R_2}{\gamma g_m} + S\frac{\alpha_N\beta_NC_2R_2}{\gamma g_mR_1} + \alpha_P\beta_P} \quad (18)$$

$$f_o = \frac{1}{2\pi}\sqrt{\frac{g_m\alpha_P\beta_P}{C_1C_2R_2}} \quad (19)$$

$$Q = R_1\alpha_N\beta_N\sqrt{\frac{\alpha_P\beta_P\gamma g_mC_1}{C_2R_2}} \quad (20)$$

$$\frac{I_{LP}}{I_{in}} = \frac{-\alpha_N\beta_N}{\frac{S^2C_1C_2R_1}{\gamma g_m} + SC_2R_1 + \alpha_N'\beta_N} \quad (21a)$$

$$\frac{I_{HP}}{I_{in}} = \frac{-\frac{S^2C_1C_2R_1}{\gamma g_m}}{\frac{S^2C_1C_2R_1}{\gamma g_m} + SC_2R_1 + \alpha_N'\beta_N} \quad (21b)$$

$$\frac{I_{BP}}{I_{in}} = \frac{\frac{\gamma'}{\gamma S C_2 R_1}}{\frac{S^2 C_1 C_2 R_1}{\gamma g_m} + S C_2 R_1 + \alpha_N' \beta_N} \quad (21c)$$

$$f_o = \frac{1}{2\pi}\sqrt{\frac{\gamma g_m \alpha_N' \beta_N}{C_1 C_2 R_1}} \quad (22)$$

$$Q = \sqrt{\frac{\alpha_N' \beta_N C_1}{g_m \gamma C_2 R_1}} \quad (23)$$

The sensitivity analysis of both the VM and CM universal filters is also carried out. The Equations 24-26 give the active and passive sensitivities of the VM filter and Equations 27-28 present the sensitivities of the CM filter.

$$S_{\alpha_P}^{\omega} = S_{\beta_P}^{\omega} = S_{\gamma}^{\omega} = S_{g_m}^{\omega} = -S_{C_1}^{\omega} = -S_{C_2}^{\omega} = -S_{R_2}^{\omega} = \frac{1}{2} \quad (24)$$

$$S_{R_1}^{Q} = S_{\beta_N}^{Q} = S_{\alpha_N}^{Q} = 1 \quad (25)$$

$$S_{\alpha_P}^{Q} = S_{\beta_P}^{Q} = S_{C_1}^{Q} = S_{\gamma}^{Q} = S_{g_m}^{Q} = -S_{C_2}^{Q} = -S_{R_2}^{Q} = \frac{1}{2} \quad (26)$$

$$S_{\alpha_N'}^{\omega} = S_{\beta_N}^{\omega} = S_{\gamma}^{\omega} = S_{g_m}^{\omega} = -S_{C_1}^{\omega} = -S_{C_2}^{\omega} = -S_{R_1}^{\omega} = \frac{1}{2} \quad (27)$$

$$S_{\alpha_N'}^{Q} = S_{\beta_N}^{Q} = S_{C_1}^{Q} = -S_{\gamma}^{Q} = -S_{g_m}^{Q} = -S_{C_2}^{Q} = -S_{R_1}^{Q} = \frac{1}{2} \quad (28)$$

It can be seen that the active and passive sensitivities are not greater than one which is desirable.

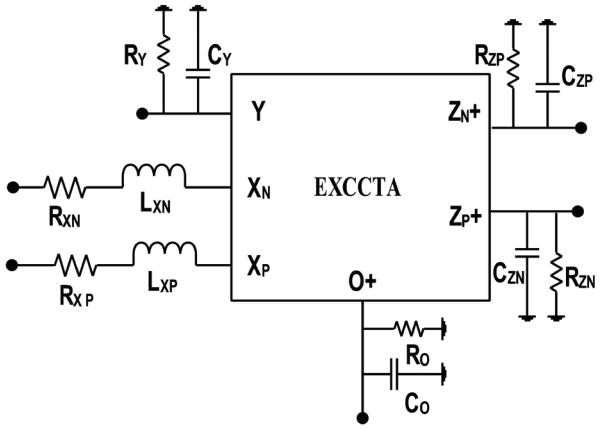

Figure 6: Non-ideal model of EXCCTA

5 Simulation results

In order to establish the workability of the proposed extra X current conveyor transconductance amplifier (EXCCTA). It was designed in 0.18µm parameters from TSMC. The circuit was simulated in spice to measure the important design metrics. The aspect ratios of the transistors are given in Table 5. The supply voltages are kept at V_{DD} = -V_{SS} = *0.9V*. The bias current was fixed at I_{bias} = 100µA. The bias current of OTA was set at 60µA which resulted in a transconductance of g_m = 0.334mS. The performance parameters of the EXCCTA are summarised in Table 6.

Table 5: Aspect ratios of the transistors

Transistor	Width (W µm)	Length(L µm)
M1- M4	3.06	0.72
M5- M7	9	0.72
M9- M23	14.4	0.72
M24- M28	0.72	0.72
M29-M32	3.6	1.8
M33-M40	7.2	1.8

The operation of the inductor simulators is evaluated next. The GIS-1 inductor simulator is tested, the passive component values are selected as R_1 = R_2 = 4kΩ, C_1 =

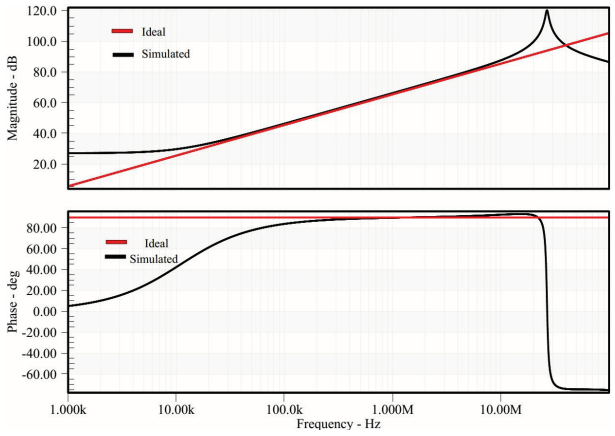

Figure 7: Magnitude and phase response of GIS-1

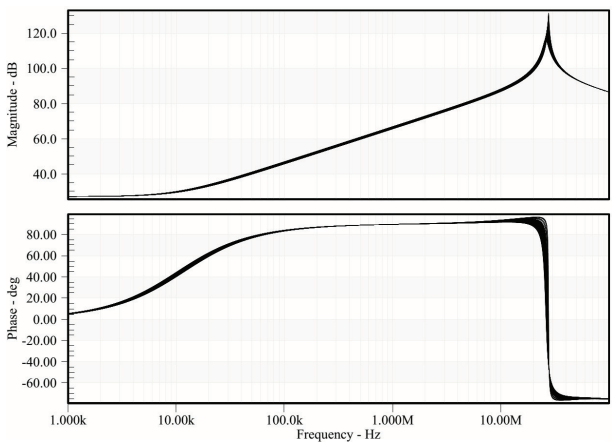

Figure 8: Monte Carlo result of GIS-1for 10% deviation in capacitance value

Table 6: Performance metrics of EXCCTA in Fig. 6

Voltage Gain	1.005
Current Gain (I_{ZP+} / I_{XP}), (I_{ZN+} / I_{XN}),	0.9998
Current Gain(I_{ZP-} / I_{XP}), (I_{ZN-} / I_{XN}),	0.964
Voltage Transfer Bandwidth	756.83MHz
Current Transfer Bandwidth (Z_{P+}, Z_{N+})	774.46 MHz
Current Transfer Bandwidth (Z_{P-}, Z_{N})	711.21 MHz
DC Voltage Range	±650mV
DC Current Range (Z_P,Z_N)	±140µA
DC Current Range (Z_{P-}, Z_{N-})	±60µA
X Node Impedance (RX)	39.940Ω
X Node Inductance (LX)	2.285µH
(Z_P,Z_N) Node Impedance	186.547kΩ
(Z_{P-}, Z_{N-}) Node Impedance	176.554kΩ

50pF and I_{bias} = 60µA resulting in the inductance of L_{eg} = 0.3mH. The magnitude response of the ideal and simulated inductor is given in Fig. 7. To study the effect of process variability on the performance of the inductor simulator Monte Carlo analysis is performed for 10% variation in the capacitance value with Gaussian distribution for 100 runs. It can be inferred from Fig. 8 that there is only slight deviation in the inductance value. To further ascertain the inductor's performance transient analysis is performed to verify the phase difference between current and voltage waveforms. The phase difference was found to be 87.2° as given in Fig. 9 which further verifies the behaviour of the synthetic inductor.

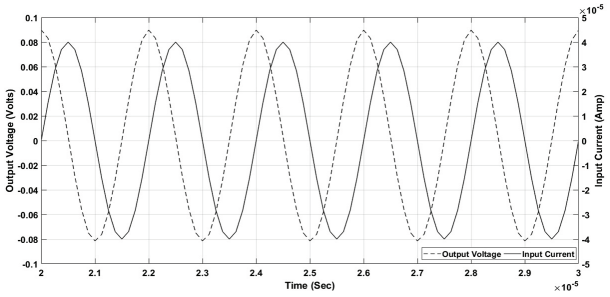

Figure 9: Transient analysis of GIS-1

The parallel inductor is now designed. The value of the passive elements are selected as $R_1 = R_1 = 4k\Omega$, $C_1 = 50pF$ and $I_{bias} = 60\mu A$ resulting in the inductance of $L_{eq} = 0.3mH$ in parallel with $R_{eq} = 4k\Omega$. It is to be noted that by appropriately selecting the value of R_1 the value of parallel resistor can be set without affecting the inductance. The magnitude response of GIS-3 is given in Fig. 10.

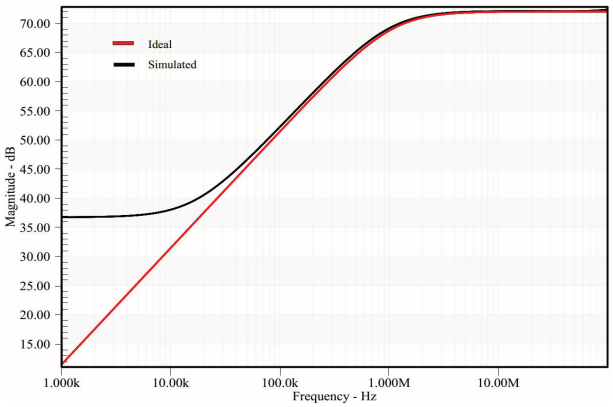

Figure 10: Magnitude response of GIS-3

6 Applications of the proposed inductance simulators

To examine the applicability and feasibility of the proposed inductor simulators in practical applications they are utilized in numerous applications. The pure inductor simulator GIS-1 is utilized in the design of third order Butterworth ladder filter [5] as shown in Fig. 11. The transfer function of the filter is given in Equation 29. The passive elements of the filter are selected as $C_1 = C_2 = 0.1$ nF, R_s = 1kΩ, R_L = 1kΩ and L_1 = 60 uH. The resistors R_s and R_L are the source and load resistances, respectively. The inductor in the passive implementation is replaced by the active GIS-1 Fig 3(a). The components of GIS-1 are selected as $R_1 = R_2 = 4k\Omega$ and C_1 = 10 pF to get L_{eq} = 60uH for the active inductor. The Ideal and simulated filter response are given in Fig.12. It can be deduced that the ideal and simulated curves bear close resemblance.

A current mode multifunction filter [27] is also designed using the GIS-1. The parallel passive RLC filter is shown in Fig. 13. The filter is designed for -3dB cutoff frequency of 2.054 MHz by selecting components values as C_f = 10pF, R_f = 10kΩ and L_{eq} = 0.6 mH. The pas-

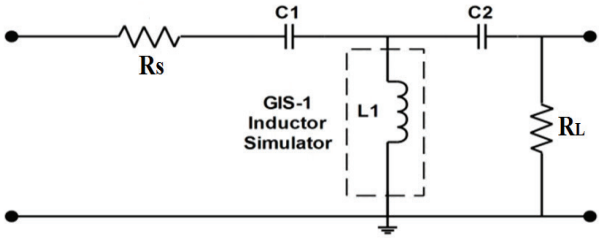

Figure 11: The third order Butterworth filter

$$\frac{V_{out}}{V_{in}} = \frac{\frac{S^3 R_L}{R_S+R_L}}{S^3+S^2\frac{Leq(C_1+C_2)+C_1C_2R_SR_L}{LeqC_1C_2(R_S+R_L)}+S\frac{C_1R_S+C_2R_L}{LeqC_1C_2(R_S+R_L)}+\frac{1}{LeqC_1C_2(R_S+R_L)}} \quad (29)$$

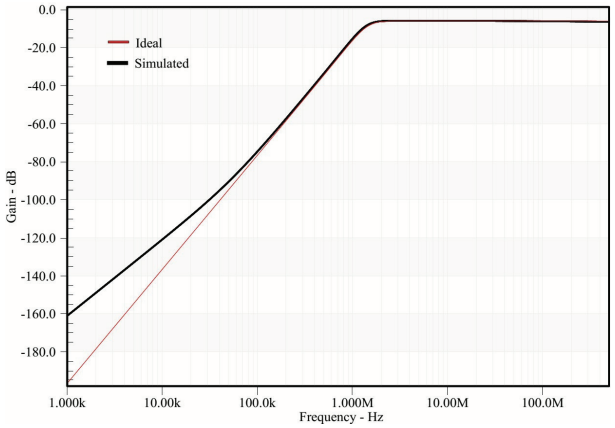

Figure 12: The response of third order Butterworth filter

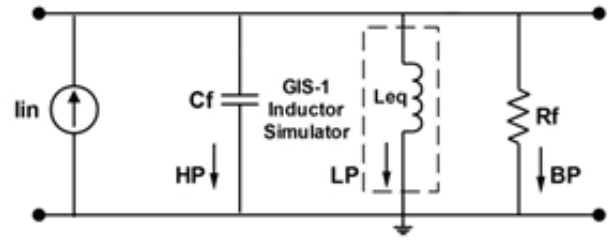

Figure 13: Current mode multi function filter

sive inductor in the filter is replaced by active inductor GIS-1. The components of GIS-1 Fig. 3(a) are selected as $R_1 = R_2 = 4k\Omega$ and $C_1 = 100$ pF to get $L_{eq} = 0.6$ mH. The ideal and simulated frequency response of the filter is given in Fig. 14.

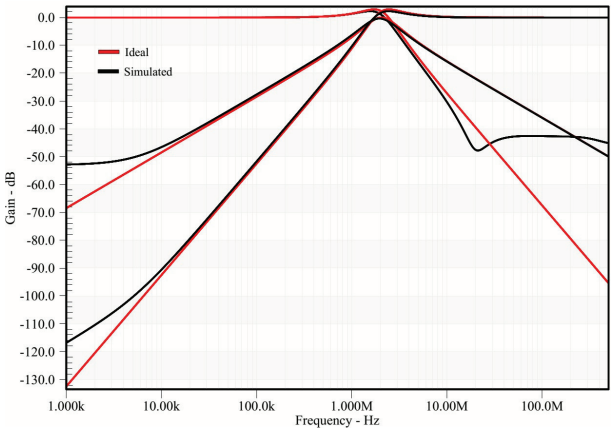

Figure 14: Frequency response of current mode multi function filter

$$f_o = \frac{1}{2\pi\sqrt{L_{eq}C_f}} \tag{30}$$

The two passive elements based inductor simulator GIS-3 is utilized in the design of voltage mode second order high pass filter as presented in Fig. 15. The transfer function and expression for frequency of the filter are given in Equations 31-32. The passive element values for the passive filter are selected as $C_f = 80$ pF, $R_f = 2k\Omega$ and $L_{eq} = 0.6$ mH which corresponds to -3dB cutoff frequency of 726.439kHz. To realize the required inductance the passive elements of the GIS-3 Fig. 3(c) are chosen to be $R_1 = 4k\Omega$ and $C_1 = 100$ pF to get L=0.6mH for GIS-3. The ideal and simulated response of the filter are given in Fig. 16.

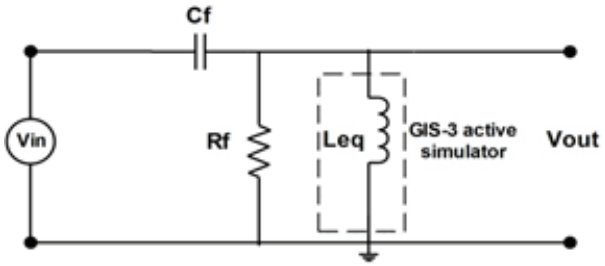

Figure 15: Voltage mode HP filter

$$\frac{V_{out}}{V_{in}} = \frac{S^2}{S^2 + S\dfrac{1}{C_f R_f} + \dfrac{1}{L_{eq}C_f}} \tag{31}$$

$$f_o = \frac{1}{2\pi\sqrt{L_{eq}C_f}} \tag{32}$$

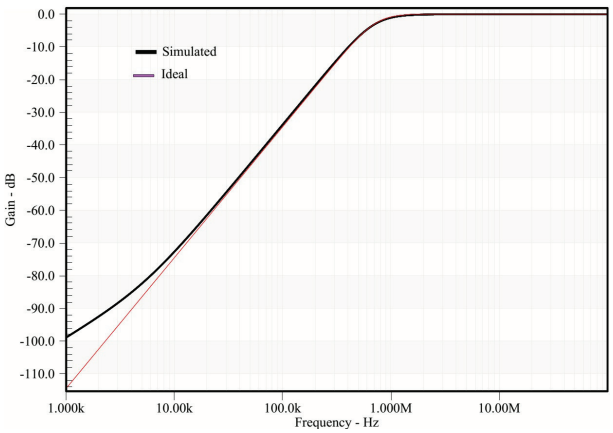

Figure 16: Frequency response of Voltage mode filter

Now the lossy parallel RL inductor GIS-4 is used in the design of second order current mode HP filter. The passive prototype of the filter is presented in Fig. 17 and the transfer function and pole frequency is given in Equations 33-34. The filter is designed for -3dB cutoff frequency of 918.88 kHz by choosing $C_f = 50$ pF, $R_{eq} = 4k\Omega$ and $L_{eq} = 0.6$ mH. The parallel $R_{eq}\|L_{eq}$ in the passive prototype are replaced by parallel RL active inductor simulator GIS-4 Fig.3 (d). The GIS-4 is designed with $R_1 = R_2 = 4k\Omega$ and $C_1 = 100$ pF. The ideal and simulated values are given in Fig. 18. To test the signal processing

capability of the filter transient analysis is performed. A sinusoidal current signal with 80μA p-p is applied to both filters with ideal passive elements and filter with simulated RL. The results are shown in Fig. 19. It is clear that the ideal and simulated curves follow each other closely verifying the correct functioning of the GIS-4 simulator.

$$\frac{I_{out}}{I_{in}} = \frac{S^2}{S^2 + S\frac{1}{C_f R_f} + \frac{1}{L_{eq} C_f}} \tag{33}$$

$$f_o = \frac{1}{2\pi\sqrt{L_{eq} C_f}} \tag{34}$$

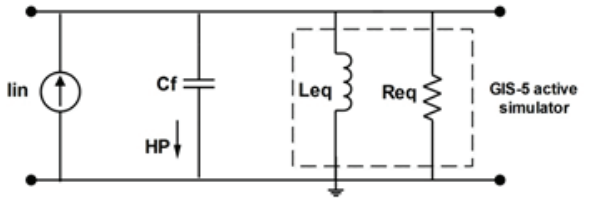

Figure 17: Current mode high pass filter

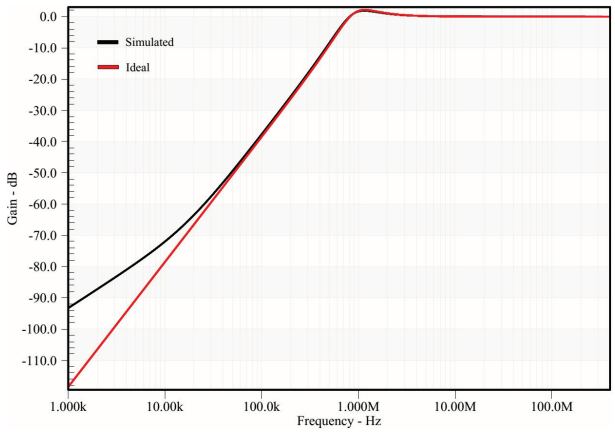

Figure 18: Frequency response of Current mode high pass filter

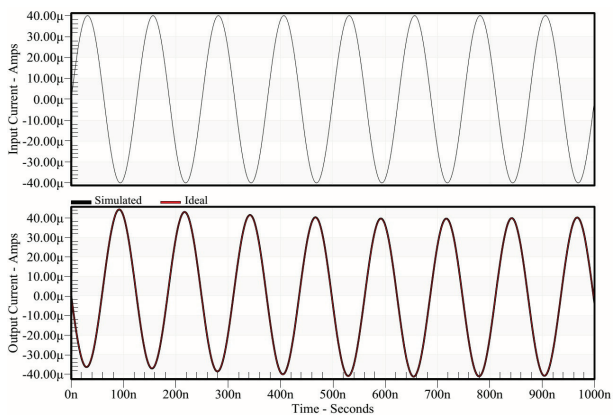

Figure 19: Transient analysis of Current mode high pass filter

7 Verification of the Proposed Universal Filters

The proposed MISO VM filter is tested. The filter is designed for -3dB cutoff frequency of 2.054MHz by selecting C_1 = 20 pF, C_2 = 20 pF, R_1 = 5kΩ and R_2 = 5kΩ. The resulting quality factor of the filter is found to be 1.29. The response of the filter is presented in Fig. 20. The response of the AP filter is given in Fig. 21. The simulated pole frequency of the is found to be 1.998MHz which translates in to 3.21% error this is due to parasitic elements discussed above. To investigate the signal processing capabilities of the filter transient analysis is also performed for the BP configuration. It can be inferred from the Fig. 22 that the filter performs well. The total harmonic distortion(THD) of the filter for band pass configuration is also calculated which is found to be perfectly within acceptable limit for wide input voltage range as shown in Fig. 23. The THD remains within 1% till 200mV input voltage.

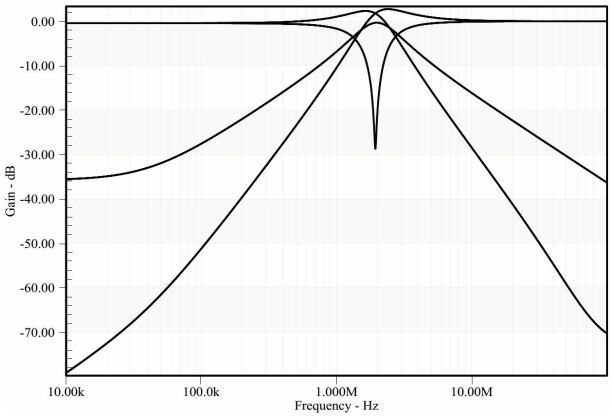

Figure 20: Simulated characteristics of the MISO VM filter

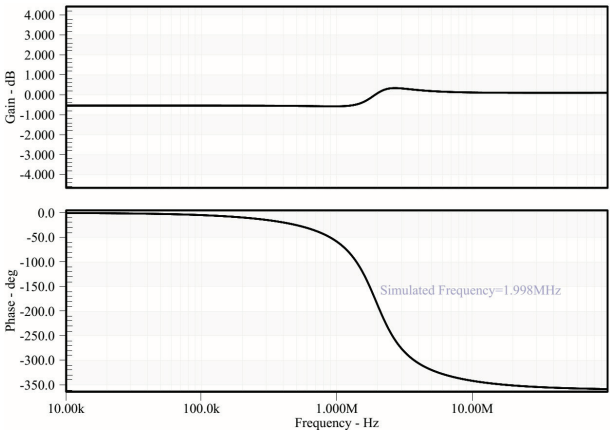

Figure 21: Simulated characteristics of the MISO VM AP filter

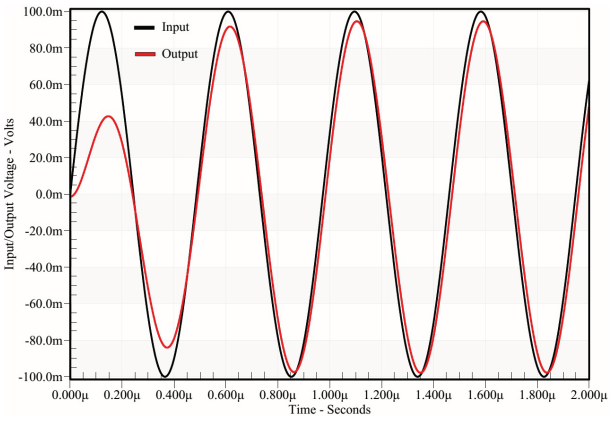

Figure 22: Transient analysis of the band pass filter

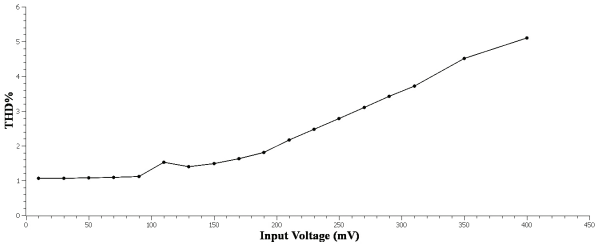

Figure 23: Total harmonic distortion of the band pass filter configuration

The effect of process variations on the proposed filter is studied by performing Monte Carlo analysis of the HP response of the filter. The analysis is carried out for 10% deviation in the two capacitor values adopting the Gaussian distribution. The result for 50 runs given in Fig. 24 shows that the filter functions well with minute deviations that can be accommodated by adjusting the bias current of the OTA for precise frequency control.

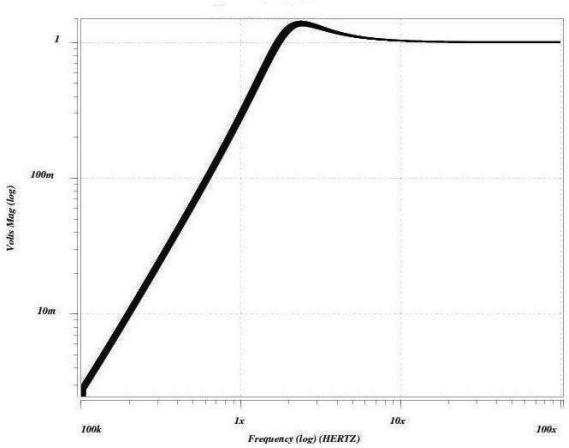

Figure 24: Monte Carlo analysis of the HP filter for 10% deviation in capacitance values

Table 7: Comparison of MISO filters available in the literature with the proposed filter

S. No.	Type of Filter	Active Block Used(No.)	No. of R+C	No. of grounded C+R	Matching Condition	Electronic Tunability	Inverting Input Needed	Low output Impedance
[29]	MISO (VM)	CCII+ (3)	2+2	0+0	No	No	No (Except for AP)	No
[30]	MISO (VM)	DVCC (3)	4+2	2+3	No (Except for AP)	No	No	No
[31]	MISO (VM)	CCTA (1)	2+2	0+0	No	Yes	No	No
[32]	MIMO (VM)	DVCC (1)	2+2	0+0	Yes	No	No	No
[33]	MISO (VM)	DOCCCII (2)	0+2	0+0	No	Yes	No (Except for AP)	No
[34]	MISO (VM)	VD-DIBA	1+2	0+0	No	Yes	No	No
[35]	MISO (VM)	CDBA (2)	4+2	0+0	Yes	No	No	Yes
[36]	MISO (VM)	DDCC (2)	2+2	2+1	No	No	No	No
[37]	MIMO (VM)	FDCCII (1)	3+2	1+1	No	No	No (Except for AP)	No
[38]	MISO (VM)	DDCC (3)	2+2	2+2	No	No	No	Yes
Proposed	MISO (VM)	EXCCTA (1)	2+2	1+0	No	Yes	No (Except for AP)	Yes

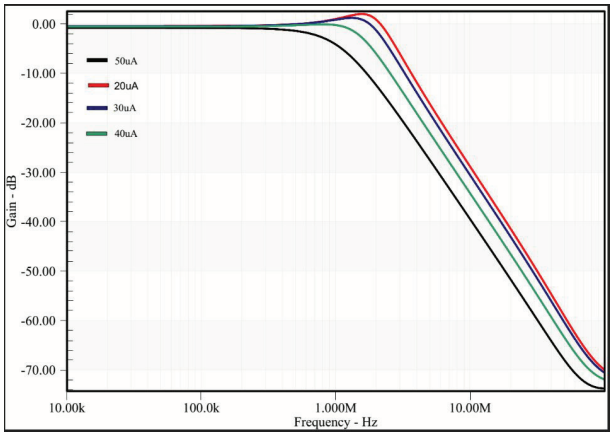

Figure 25: Simulated characteristics of the MISO VM LP filter for different bias currents

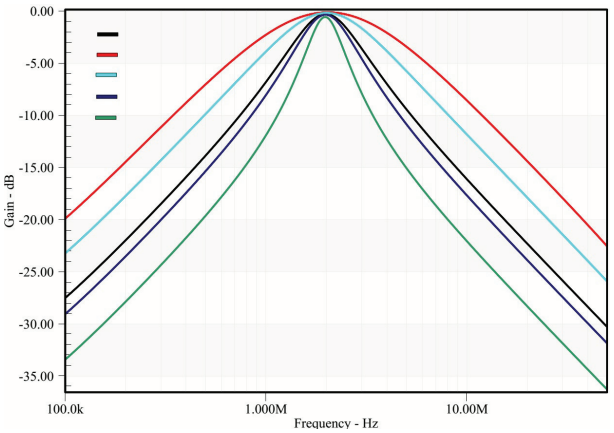

Figure 26: Simulated characteristics of the MISO VM BP filter for different quality factors

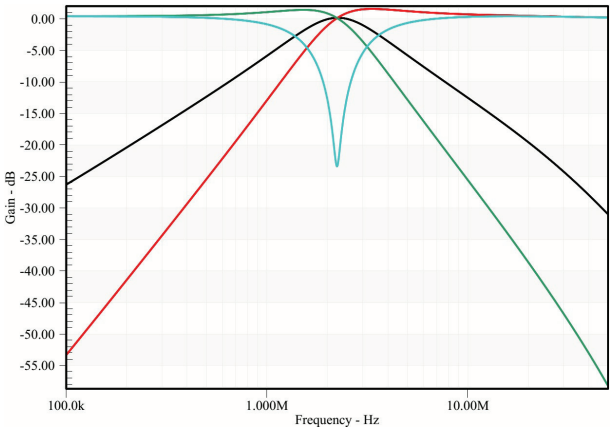

Figure 27: Simulated characteristics of the SIMO CM filter

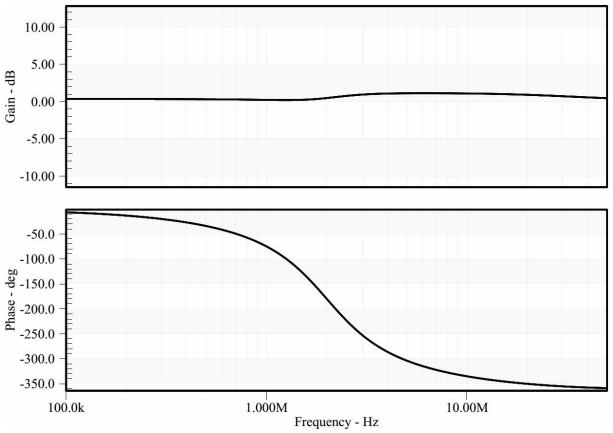

Figure 28: Simulated characteristics of the SIMO CM AP filter

Tunability is an importance feature of filters [28], this attribute enables a filter to be useful at different frequencies without requiring any alteration in the passive components values. The pole frequency of the proposed filter can be adjusted by varying the bias current of the OTA. The LP response of the filter is plotted for different bias currents as shown in Fig. 25. It can be seen from the figure that the bias current slightly effects the quality factor of the filter as can be deduced from Equations (13-14) . To realize a unity quality factor the resistance R_1 should be adjusted accord-

Table 8: Comparison of CM SIMO filters available in the literature with the proposed filter

S. No.	Type of Filter	Active Block Used(No.)	No. of R+C	No. of grounded C+R	Matching Condition	Electronic Tunability	High output Impedance
[39] Fig. 3	SIMO (CM)	CBTA (1)	2+2	2+2	No	Yes	No
[40]	SIMO (CM)	CDTA (1)	2+2	2+0	No	Yes	No
[41]	SIMO (CM)	DV-DXCCI (1)	2+2	2+2	No	No	Yes
[42]	SIMO (CM)	UCC (3)	2+2	2+2	No	No	Yes
[43]	SIMO (CM)	CCCII (3)	0+2	2+0	No	Yes	Yes
Proposed	SIMO (CM)	EXCCTA (1)	1+2	1+2	No	Yes	Yes

ingly. The quality factor of the proposed filter can also be tuned independent of the pole frequency by varying the resistance R_1 as can be seen in Figure 26 which gives the plot of Q for different values of resistance R_1.

A comparison is provided in Table 7 to compare the proposed VM MISO filter with the other state of the art filter structures.

Lastly, the CM SIMO filter is validate by designing it for -3dB cutoff frequency of 2.204MHz by selecting C_1 = 20 pF, C_2 = 20 pF, R_1 = 3.61 kΩ and OTA bias current of 50µA. The frequency response of the filter is given in Fig. 27 and the AP response is shown in Fig. 28 The filter is compared with other exemplary SIMO filter topologies to highlight its advantages as shown in Table 8.

8 Experimental Results

The EXCCTA can be easily implemented using commercially available integrated circuits AD844 and LM13700. The possible implementation of GIS-1 using only two AD844 and one LM13700 IC is shown in Fig. 29. The ICs are supplied with a bias voltage of ±10V, the I_{bias} of the OTA is fixed at 372µA. The passive components values are chosen to be R_1 = R_2 =1kΩ and C_1 = 10 nF resulting in the inductance of L=672µH. To test the circuit a triangular waveform with 2V p-p at 17kHz is applied through R_2 and R_3 to convert it in to corresponding input triangular current. A square wave form is obtained across the inductor. The oscilloscope output is shown in Fig. 30 which validates the correct functioning of the active inductor.

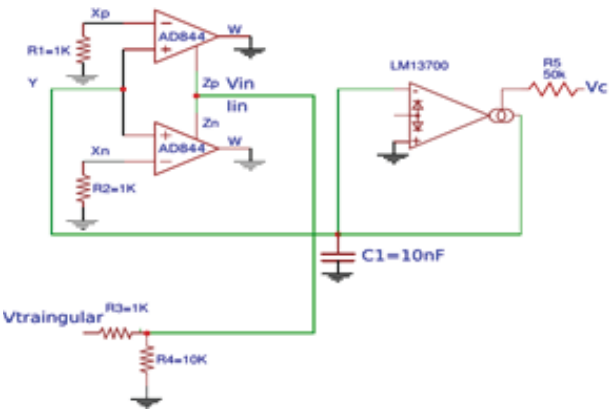

Figure 29: Implementation of the GIS-1 from the commercially available ICs

To further validate the VM filter it is implemented on breadboard using AD844 and LM13700 ICs. The filter implementation is given in Fig. 31 (a-b). The filter is designed for -3dB frequency of 343.199kHz by selecting

Figure 30: The experimental result of the inductor simulator

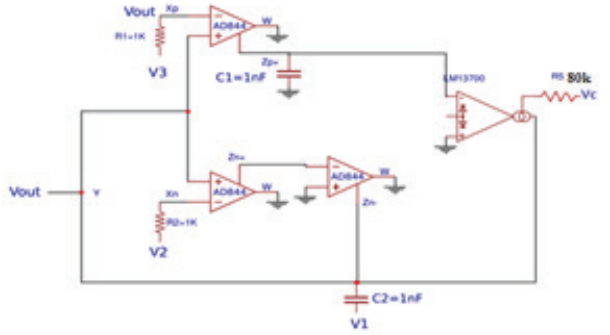

(a)

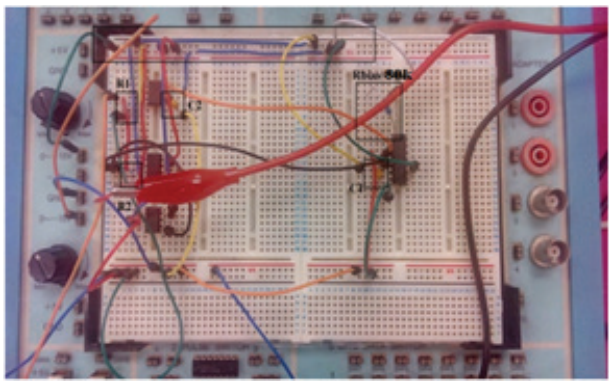

(b)

Figure 31: Experimental setup of the VM filter from the commercially available ICs (a) Block Diagram (b) Bread board implementation

passive components values equal to R_1 = R_2 =1kΩ, C_1 = C_2 =1nF and I_{bias} = 232.5µA. The ideal and experimentally calculated response of the filter is presented in Fig. 32. The measured frequency of the filter is found to be 321kHz leading to an error of 6.46%, this discrepancy arises due to non-idealities present in the EXCCTA and also due to the parasitics introduced by connecting leads and breadboard, nonetheless it verifies the practical feasibility of the proposed VM filter.

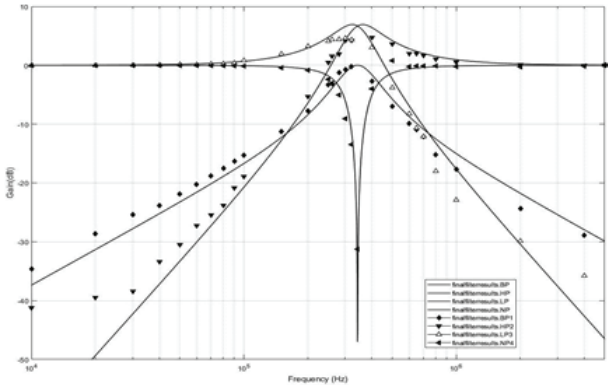

Figure 32: The ideal and experimental results of the VM MISO filter

(a)

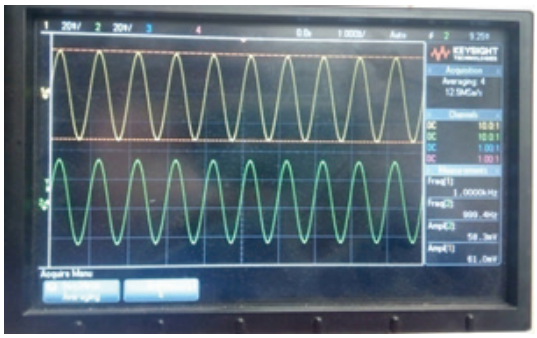

(b)

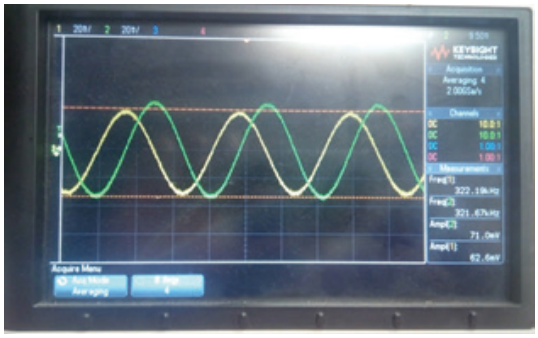

(c)

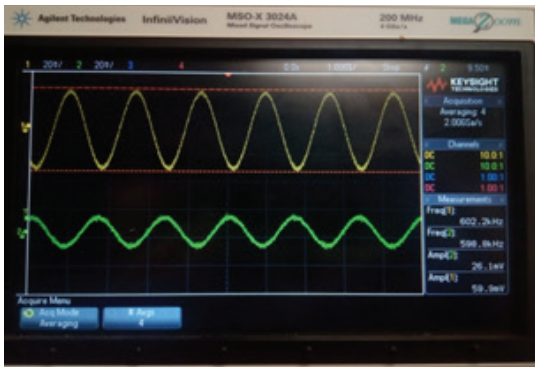

Figure 33: Time domain analysis of LP response (a) 1kHz (b)321 kHz (c) 600 kHz

The experimental time domain analysis of the filter is also performed by exciting it with a sinusoidal input signal of 60mV p-p at frequencies of 1kHz, 321kHz and 600kHz. The filter output obtained on the oscilloscope for LP configuration is presented in Fig. 33 (a-c).

9 Conclusion

In this research, a new active element namely EXCCTA is proposed. The EXCCTA is used to design six topologies of lossy and lossless active inductors. Additionally, to further elaborate its versatility two universal VM and CM filter structures employing a single EXCCTA are also proposed. The inductor simulators make use of single EXCCTA, grounded passive elements, requires no passive components matching and are perfectly tunable. The voltage mode filter is obtained by slightly modifying the proposed series inductor. The VM filter makes use of canonical number of passive elements and has low output impedance. The CM filter is SIMO type and utilize only three grounded passive elements for implementation. Both the proposed filter structures enjoy low sensitivities, inbuilt tunability and orthogonal control of quality factor and pole frequency. The non-ideal analysis of the inductor simulators and filter structures is also performed. The simulations are performed in 0.18µm parameters from TSMC to verify the theoretical analysis. Experimental results for pure inductor and SIMO VM filter are also included to substantiate the theoretical findings.

10 Acknowledgement

The authors gratefully acknowledge the support provided by UKM internal grant (GUP-2015-021) for this study.

11 Reference

1. İbrahim, M. A., Minaei, S., Yüce, E., Herencsar, N., & Koton, J. (2012). Lossy/lossless floating/grounded inductance simulation using one DDCC.
2. Yuce, E. (2006). Floating inductance, FDNR and capacitance simulation circuit employing only grounded passive elements. *International Journal of Electronics*, *93*(10), 679-688.
3. Metin, B., & Cicekoglu, O. (2006). A novel floating lossy inductance realization topology with NICs using current conveyors. *IEEE Transactions On Circuits And Systems II: Express Briefs*, *53*(6), 483-486.
4. Cicekoglu, M. O. (1998). Active simulation of grounded inductors with CCII+ s and grounded passive elements. *International Journal of Electronics*, *85*(4), 455-462.

5. Alpaslan, H., & Yuce, E. (2015). Inverting CFOA based lossless and lossy grounded inductor simulators. *Circuits, Systems, and Signal Processing*, *34*(10), 3081-3100.
6. Ferri, G., & Guerrini, N. C. (2003). *Low-voltage low-power CMOS current conveyors*. Springer Science & Business Media.
7. Mohan, P. A. (2012). *Current-mode VLSI analog filters: design and applications*. Springer Science & Business Media.
8. Alzaher, H. A. (2008). A CMOS digitally programmable universal current-mode filter. *IEEE Transactions on Circuits and Systems II: Express Briefs*, *55*(8), 758-762.
9. Van Valkenburg, M. E. (1982). *Analog filter design* (pp. 136-137). Holt, Rinehart, and Winston.
10. Pathak, J. K., Singh, A. K., & Senani, R. (2016). New canonic lossy inductor using a single CDBA and its application. *International Journal of Electronics*, *103*(1), 1-13.
11. Metin, B. (2012). Canonical inductor simulators with grounded capacitors using DCCII. *International Journal of Electronics*, *99*(7), 1027-1035.
12. Pandey, R., Pandey, N., Paul, S. K., Singh, A., Sriram, B., & Trivedi, K. (2011). New topologies of lossless grounded inductor using OTRA. *Journal of Electrical and Computer Engineering*, *2011*, 7.
13. Yuce, E., & Minaei, S. (2017). Commercially Available Active Device Based Grounded Inductor Simulator and Universal Filter with Improved Low Frequency Performances. *Journal of Circuits, Systems and Computers*, *26*(04), 1750052.
14. Metin, B., Herencsar, N., Koton, J., & Horng, J. W. (2014). DCCII-based novel lossless grounded inductance simulators with no element matching constrains. *Radioeng J*, *23*, 532-4538.
15. Çam, U., Kaçar, F., Cicekoglu, O., Kuntman, H., & Kuntman, A. (2003). Novel grounded parallel immittance simulator topologies employing single OTRA. *AEU-International Journal of Electronics and Communications*, *57*(4), 287-290.
16. Yuce, E., Minaei, S., & Cicekoglu, O. (2005). A novel grounded inductor realization using a minimum number of active and passive components. *Etri Journal*, *27*(4), 427-432.
17. Yuce, E., Minaei, S., & Cicekoglu, O. (2006). Limitations of the simulated inductors based on a single current conveyor. *IEEE Transactions on Circuits and Systems I: Regular Papers*, *53*(12), 2860-2867.
18. Yuce, E., & Minaei, S. (2008). A modified CFOA and its applications to simulated inductors, capacitance multipliers, and analog filters. *IEEE Transactions on Circuits and Systems I: Regular Papers*, *55*(1), 266-275.
19. Yuce, E. (2009). Novel lossless and lossy grounded inductor simulators consisting of a canonical number of components. *Analog Integrated Circuits and Signal Processing*, *59*(1), 77-82.
20. Yuce, E., & Minaei, S. (2009). On the realization of simulated inductors with reduced parasitic impedance effects. *Circuits, Systems, and Signal Processing*, *28*(3), 451-465.
21. Kumar, P., & Senani, R. (2010). New grounded simulated inductance circuit using a single PFTFN. *Analog Integrated Circuits and Signal Processing*, *62*(1), 105.
22. Kaçar, F., & Yeşil, A. (2010). Novel grounded parallel inductance simulators realization using a minimum number of active and passive components. *Microelectronics Journal*, *41*(10), 632-638.
23. Gupta, A., Senani, R., Bhaskar, D. R., & Singh, A. K. (2012). OTRA-based grounded-FDNR and grounded-inductance simulators and their applications. *Circuits, Systems, and Signal Processing*, *31*(2), 489-499.
24. Kacar, F., & Kuntman, H. (2011). CFOA-based lossless and lossy inductance simulators. *Radioengineering*, *20*(3), 627-631.
25. Kaçar, F., Yeşil, A., Minaei, S., & Kuntman, H. (2014). Positive/negative lossy/lossless grounded inductance simulators employing single VDCC and only two passive elements. *AEU-International Journal of Electronics and Communications*, *68*(1), 73-78.
26. Maheshwari, S. (2013). Current conveyor all-pass sections: brief review and novel solution. *The Scientific World Journal*, *2013*.
27. Senani, R. (1996). A simple approach of deriving single-input-multiple-output current-mode biquad filters. *Frequenz*, *50*(5-6), 124-127.
28. Faseehuddin, M., Sampe, J., Shireen, S., & Ali, S. H. M. (2017). A Novel Mix-Mode Universal Filter Employing a Single Active Element and Minimum Number of Passive Components. *Informacije MIDEM*, *47*(4), 211-222.
29. Horng, J. W. (2001). High-input impedance voltage-mode universal biquadratic filter using three plus-type CCIIs. *IEEE Transactions on Circuits and Systems II: Analog and Digital Signal Processing*, *48*(10), 996-997.
30. Horng, J. W., Hsu, C. H., & Tseng, C. Y. (2012). High input impedance voltage-mode universal biquadratic filters with three inputs using three CCs and grounding capacitors. *Radioengineering*, *21*(1), 290-296.
31. Herencsar, N., Koton, J., & Vrba, K. (2009). Single CCTA-Based Universal BiquadraticFilters Employing Minimum Components. *International Journal of Computer and Electrical Engineering*, *1*(3), 307.
32. Horng, J. W., & Jhao, Z. Y. (2013). Voltage-mode universal biquadratic filter using single DVCC. *ISRN Electronics*, *2013*.

33. Ranjan, A., & Paul, S. K. (2011). Voltage mode universal biquad using CCCII. *Active and Passive Electronic Components*, *2011*.
34. Pushkar, K. L., Bhaskar, D. R., & Prasad, D. (2013). A new MISO-type voltage-mode universal biquad using single VD-DIBA. *ISRN Electronics*, *2013*.
35. Pathak, J. K., Singh, A. K., & Senani, R. (2013). New voltage mode universal filters using only two CD-BAs. *ISRN Electronics*, *2013*.
36. Chang, C. M., & Chen, H. P. (2003). Universal capacitor-grounded voltage-mode filter with three inputs and a single output. *International Journal of Electronics*, *90*(6), 401-406.
37. Chang, C. M., & Chen, H. P. (2005). Single FDCCII-based tunable universal voltage-mode filter. *Circuits, Systems, and Signal Processing*, *24*(2), 221-227.
38. Chiu, W. Y., & Horng, J. W. (2007). High-input and low-output impedance voltage-mode universal biquadratic filter using DDCCs. *IEEE Transactions on Circuits and Systems II: Express Briefs*, *54*(8), 649-652.
39. Sagbas, M., Ayten, U. E., & Sedef, H. (2010). Current and voltage transfer function filters using a single active device. *IET circuits, devices & systems*, *4*(1), 78-86.
40. Prasad, D., Bhaskar, D. R., & Singh, A. K. (2009). Universal current-mode biquad filter using dual output current differencing transconductance amplifier. *AEU-International Journal of Electronics and Communications*, *63*(6), 497-501.
41. Beg, P., & Maheshwari, S. (2014). Generalized filter topology using grounded components and single novel active element. *Circuits, Systems, and Signal Processing*, *33*(11), 3603-3619.
42. Jerabek, J., & Vrba, K. (2010). SIMO type low-input and high-output impedance current-mode universal filter employing three universal current conveyors. *AEU-International Journal of Electronics and Communications*, *64*(6), 588-593.
43. Wang, C., Liu, H., & Zhao, Y. (2008). A new current-mode current-controlled universal filter based on CCCII (±). *Circuits, Systems, and Signal Processing*, *27*(5), 673-682.

Arrived: 18. 12. 2017
Accepted: 04. 05. 2018